Evidence of the early stage of porphyrin aggregation by enhanced Raman scattering and fluorescence spectroscopy

Norberto Micali* and Valentina Villari
Istituto per i Processi Chimico-Fisici, CNR, Via La Farina 237, I-98123, Messina, Italy

Andrea Romeo, Maria Angela Castriciano, and Luigi Monsù Scolaro
Dipartimento di Chimica Inorganica, Chimica Analitica e Chimica Fisica and CIRCMSB, Università di Messina Salita Sperone 31, I-98166 Villagio S. Agata, Messina, Italy

(Received 14 May 2007; published 18 July 2007)

The early stage of fractal porphyrin diffusion-limited aggregation (DLA), induced by addition of a polyamine, is observed in aqueous solution by enhanced Raman scattering and fluorescence quenching. The enhancement of Raman scattering is due to nonlinear optical properties typical of fractal composites. Although this early stage (reaction-limited aggregation) has been theoretically predicted (by mean-field theory and molecular dynamics simulation), it is experimentally difficult to observe. During this initial stage, fluorescence quenching gives direct information on the decrease of the concentration of monomeric porphyrins, whereas Raman scattering (through characteristic vibrational modes of the aggregate) reports on the concentration of porphyrins in the aggregated form. These small clusters constitute the seeds for the DLA aggregation process leading to micrometric-sized fractals.

DOI: 10.1103/PhysRevE.76.011404 PACS number(s): 61.43.Hv, 78.30.−j, 82.70.−y, 33.50.−j

I. INTRODUCTION

Porphyrins are a well-known class of organic compounds which have been widely exploited as building blocks for designing and accessing to supramolecular systems [1]. Porphyrins have the tendency to self-aggregate in dimers or higher oligomers through the occurrence of σ-π stacking interactions [2]. These molecules have been successfully applied in mimicking photosynthetic centers [3], in cancer photodynamic therapy [4], as probes for nucleic acid conformation and dynamics [5], and as materials with favorable optoelectronic properties [6]. As far as this last point is concerned, porphyrins are particularly suited because their properties can be widely modulated by the proper choice of mesosubstituents, coordinated metal ions and axial substituents. All these factors, together with thermodynamical parameters of the medium (e.g., ionic strength, *p*H, and temperature) allow for a fine control of the synthesis of new materials having specific properties and functions.

In this respect, porphyrin J-type aggregates have attracted considerable interest [7–13], due to their peculiar structural, kinetic, and photophysical properties. The water-soluble 5,10,15,20-tetrakis(4-sulfonatophenyl)porphyrin ($TPPS_4$) has been most investigated, being able to form J aggregates under acidic conditions [14,15]. The length and size of these species can be controlled by the nucleating agent [16], by exploiting microemulsions as nanoreactors [17–19], and/or in the presence of cationic templates [20]. The mesoscopic fractal structure of these porphyrin J aggregates has been previously described [14,15,20,21] and, in particular, different fractal structures (driven by different aggregation kinetics) are obtained as a function of the thermodynamic parameters of the solution [15]. According to the mean-field theory based on the von Smoluchowski equation [22] and to molecular dynamics (MD) simulations [23,24], a reaction-limited (RLA) early stage of the fractal aggregation is expected to precede the diffusion-limited aggregation (DLA) regime. A dynamic-scaling approach [25] for the cluster growth describes the cluster mass distribution as $N(M,t)=[\bar{M}(t)]^{-2}f(M/\bar{M}(t))$, where N is the number of clusters with mass M and $\bar{M}(t)$ is the average mass of clusters. The difference between RLA, and DLA regimes is based on the time dependence of $\bar{M}(t)$ and on the shape of $f(M/\bar{M}(t))$. In particular, $\bar{M}(t)$ grows exponentially for RLA whereas it follows a power law for DLA.

As an example, in the case of salt-induced aggregation of the cationic porphyrin trans-bis (N-methylpyridinium-4-yl) diphenylporphine (t-H_2Pagg), uv-visible measurements suggested the existence of this RLA stage occurring before the DLA mechanism [26]. In the case of $TPPS_4$, aggregation can also be induced by the presence of polyamines (e.g., spermine); such aggregates display nonlinear optical properties, analogous to those of metal composites. Nanostructured and fractal aggregates, especially those composites formed by metal particles, give rise to enhanced Raman and Rayleigh light scattering [27]. In these systems, the optical properties are dramatically different from those observed in nonaggregated systems: the local electric field at some nanoparticles differs significantly from the macroscopic one [28,29]. In fractal nanocomposites, which do not have translational invariance, excitations are localized in subwavelength regions, called "hot zones," whose spatial position strongly depends on the frequency of the dipolar eigenmodes of the system. Although the hot zones are localized in nanometric regions, they overall fill the cluster size, due to the simultaneous excitation of a group of eigenmodes by the external field. In other words, when the frequency of the illuminating field is close to the frequency of the dipolar eigenmodes of the sys-

*micali@me.cnr.it

tem, a strong scattering enhancement occurs. These hot zones can be experimentally measurable by near-field techniques, whereas far-field techiques like optical microscopy and micro-Raman spectroscopy give information in which the hot zones and spectral features are averaged out.

The chemical nature of the composite is taken into account in the dipole-dipole interaction only via $Z=X+i\delta=\alpha_0^{-1}$, which is the inverse of the polarizability α_0 of the monomer, whereas the amplification of the local field in the proximity of a resonant monomer, dependent on the ratio $Q=|X|/\delta$ (the quality factor of the composite), is responsible for the Rayleigh and Raman enhancement [27,30].

We have shown [31] that an aqueous solution of $TPPS_4$ in the presence of spermine can be considered as an organic nanocomposite. Enhancement of the optical properties occurs in the presence of the polyamine, which is directly involved in the formation of the fractal aggregate [31]. In particular, whereas in the absence of spermine the Frenkel exciton model [32,33] can explain the polarizability behavior satisfactorily, the addition of spermine induces structural branching through interactions between the protonated nitrogen atoms of the spermine and the negatively charged sulfonate end groups of porphyrins not involved in the porphyrin-porphyrin contacts in the J aggregate. In the composite, formed when aggregates are seeded into the spermine substrate, the dipole-dipole interaction among porphyrins (not belonging to the J aggregate) must be considered in order to explain the broadening of the absorption band, the energy shift observed experimentally, and the wavelength dependence of the scattering [31].

Therefore, in this system, beyond the enhancement of the Rayleigh scattering, Raman enhancement is also expected. Such enhancement allows for the study of the aggregate growth through the identification of its characteristic vibrations.

In the present paper, we report on a Raman, micro-Raman, and fluorescence investigation of spermine-induced aggregates of $TPPS_4$ under mild acidic conditions (pH=2.9). While the fluorescence quenching monitors the decrease of free porphyrin concentration, the enhanced Raman scattering of the composite allows for following the spectroscopic feature of the characteristic aggregate vibration peaks. Both techniques are able to identify the early RLA stage of the fractal aggregation in a complementary way.

II. PREPARATION OF THE AGGREGATED SAMPLES

Samples of aggregated diacid $TPPS_4$ (Aldrich, tetrasodium salt) were prepared by adding a known volume of a concentrated stock solution of spermine (Sigma) to an aqueous solution of porphyrin (3 μM) in 10 mM citrate buffer at the requested pH (2.9). Milli-Q water was used throughout. Samples for microscopy were prepared by slow evaporation of a droplet of the final reaction mixture (when aggregation is completed) under a dust-free atmosphere.

III. EXPERIMENTAL SECTION

The uv-visible measurements were performed by using a Hewlett-Packard model 8452A diode array spectrophotometer. Resonance light scattering (RLS) experiments were performed on a Jasco model FP-750 spectrofluorimeter using a synchronous scan protocol with a right-angle geometry [34].

The Raman spectra were collected using the 514 nm line of a spectra-physics model 2000 Ar^+ laser (with a power lower than 60 mW). In the micro-Raman configuration, the exciting beam was directed to an Olympus BX-40 microscope and focused onto the sample via a microscope objective ($\times$100). The Raman signal was collected by the same microscope objective in a backscattering configuration and analyzed through a Jobin Yvon Spex U1000 spectrometer equipped with a nitrogen-cooled charge-coupled device (Jobin Yvon Spectrum-1 B24) [35]. The fluorescence spectra were collected at 700 nm using the same equipment, exciting the sample at 488 nm.

Static light scattering measurements were performed by a standard apparatus using a home-made goniometer and an exciting 532 nm line from a Nd:yttrium aluminum garnet laser. The investigated scattering angle range was $20° \leqslant \theta \leqslant 150°$ corresponding to exchanged wave vector values $5.5 < k < 30.5\ \mu m^{-1}$ {where $k=[(4\pi n)/\lambda]\sin(\theta/2)$, with n the refractive index of the medium, λ the wavelength in vacuum, and θ the scattering angle}. The measured scattered intensity of the solution was normalized by the scattered intensity of toluene used as reference.

IV. RESULTS AND DISCUSSION

The aggregation of $TPPS_4$ is fostered by decreasing the pH below 1, where this porphyrin is in its diacid monomeric form, or greatly increasing the ionic strength [7–10,14,20,36]. We have recently observed that addition of a fairly large amount of spermine can induce the formation of J aggregates at pH$>$2.0 [31]. Indeed, when a 30-fold excess of polyamine is added to a diluted porphyrin solution at pH=2.9, the formation of a J band bathochromically shifted (492 nm) with respect to the Soret band of the diacid form (434 nm) is observed. The corresponding RLS spectra evidence an intense peak centered at 500 nm, revealing the aggregated nature of the species at 492 nm. This general pattern of behavior is strictly similar to that of the aggregates formed by $TPPS_4$ in the absence of a templating polyamine, but in the latter case a much higher concentration of acid is needed.

The main difference between the $TPPS_4$-spermine composite and the salt- or pH-induced $TPPS_4$ aggregates consists in the presence of an intense detuned extinction band (typical of composites) in the former. In contrast, the resonant scattering of the salt-or pH-induced J aggregates displays an intense narrow scattering band around the characteristic absorption wavelength of the J aggregates. In fact, in the composite, besides the exciton coupling inside the J aggregate, the porphyrin molecules (inside the aggregate) not involved in the J aggregate interact through dipolar coupling, enhancing the scattering [31].

For the $TPPS_4$-spermine composite, although RLS spectra contain information on the resonance properties of the system, they do not contain quantitative information on the scattering enhancement; indeed, whereas the scattering enhance-

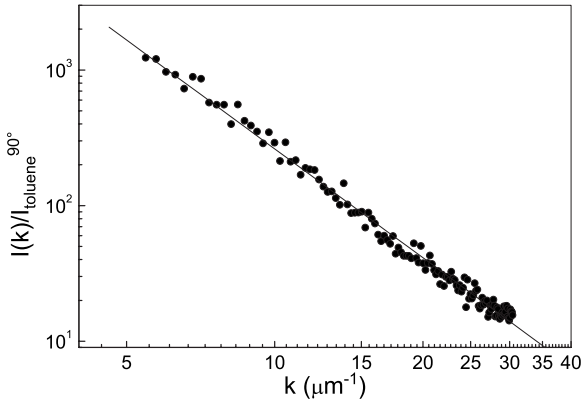

FIG. 1. Static light scattering intensity profile of the aggregated sample as a function of the exchanged wave vector. The continuous line is the fit according to the fractal power law (see text).

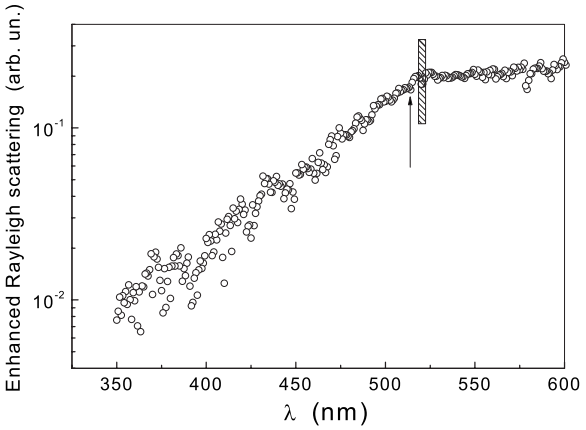

FIG. 2. Enhanced Rayleigh scattering of the aggregated sample reported in Ref. [31], as a function of the wavelength. The scattering profile of the aggregated sample of this work (analogous to that of Ref. [31]) is shown in Fig. 1. The arrow indicates the excitation wavelength and the dashed area the Stokes shift range.

ment involves the total scattering power, RLS measures only the scattering at 90°. As shown in Fig. 1, the investigated porphyrin system displays a scattered intensity which is strongly dependent on the scattering angle (and hence on the exchanged wave vector), so that RLS does not represent the spectral behavior of the enhancement.

The intensity profile of the scattered light for the aggregated porphyrin, after the aggregation is completed, follows a power law $I(k)=Ak^{-D_f}$, as shown in Fig. 1. From the slope of the straight line in this log-log plot, it is possible to derive the exponent $D_f=2.6\pm0.2$, in agreement with previous results [31]. This occurrence ensures the reproducibility of the final structure of the aggregates. According to statistical physics, this power law is a feature of the aggregation mechanism, which can be described in terms of fractal geometry. In fractal aggregates, the mass M of a cluster is related to the corresponding radius R through the scaling form $M \propto R^{D_f}$, where D_f is the fractal dimension. Theoretical models and molecular dynamics simulations relate the value of this parameter to the dynamics of the cluster growth [$D_f=2.5$, for diffusion-limited aggregation, $D_f=2.1$, for reaction-limited aggregation, and $D_f=1.75$, for diffusion limited cluster-cluster aggregation (DLCCA), etc.] [37].

The described fractal structures, governed by diffusion, are the consequence of a kinetic aggregation process described by the von Smoluchowski equation, which relates the concentration changes of the species i and j to form species $i+j$ [22]:

$$P_i + P_j \xrightarrow{K(i,j)} P_{i+j},$$

$$\frac{dc_k}{dt} = \frac{1}{2}\sum_{i+j=k} c_i K(i,j) c_j - c_k \sum_{j=1}^{\infty} K(k,j) c_j, \qquad (1)$$

where P_j denotes an aggregate containing j monomers, $K(i,j)$ is the reaction kernel of creation and destruction of the aggregate, and c_k is the concentration of the species k. In the present case, P_{i+j} is a fractal cluster, so that the reaction kernel must be a homogeneous function: $K(ai,aj)=a^{\lambda}K(i,j)$, with $\lambda \leqslant 1$ and $K(1,j)=j^{\nu}$, with $\nu \leqslant 1$ [23,37]. In this frame, for different values of the quantities λ and ν, different fractal dimensions of the aggregate are obtained. As examples, the condition $\lambda < \nu$ gives rise to DLA fractals, whereas for $\lambda > \nu$ DLCCA fractals are formed.

Our experimental findings suggest that, at the end of the aggregation kinetics (after some hours from the mixing of the reagents), porphyrins are fractally arranged according to a DLA mechanism. However, extended aggregation is detected only a couple of minutes after mixing, as evidenced by the appearance of the RLS signal and the static light scattering profile. Therefore, in order to investigate the early stage (within 60 s from mixing) of the aggregation process we performed enhanced Raman scattering, by exciting at 514 nm, where the composite has a strong enhancement of the local electric field.

The Raman scattering enhancement factor G depends on the Raman shift. For very large wavelength of Raman emission, greater than the values of the monomer absorption spectrum, it becomes $G \propto Q|X|\mathrm{Im}(\alpha)$, with α the polarizability of the aggregate. That is, the enhancement factor is due only to the local field (indeed, for large frequency shifts, the Raman photon is out of resonance). On the other hand, for small wavelength of Raman emission (close to the values of the monomer absorption spectrum), a higher enhancement occurs due to the Raman photon emitted in the resonant environment: $G \propto Q^3|X|\mathrm{Im}(\alpha)$ [30].

In Fig. 2, the enhanced Rayleigh scattering is reported, as extracted from the inset to Fig. 3 of Ref. [31]; the arrow indicates the excitation wavelength and the dashed area the Stokes shift range (180–325 cm^{-1}) containing the characteristic vibrational peaks of the aggregate. Since both the excitation wavelength and the low-frequency Stokes shifts belong to the scattering enhancement region, enhanced Raman scattering occurs. The experimental procedure adopted in Ref. [31] for obtaining the enhanced Rayleigh scattering is based on two independent measurements of absorption and extinction; their difference represents the total scattering contribution. By normalizing this difference by the scattering of the monomers constituting the aggregate, a quantity pro-

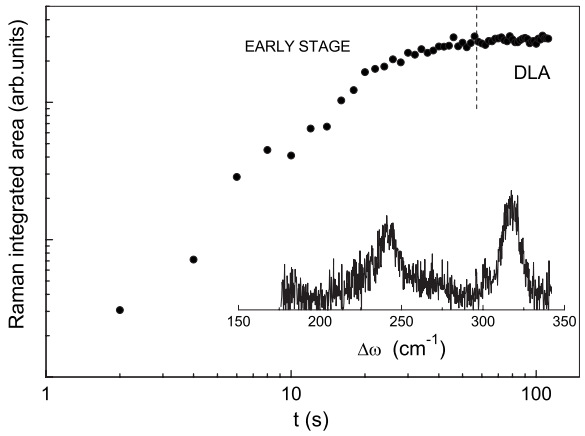

FIG. 3. Kinetic profile of the low-frequency Raman bands (integrated area of the peaks at 242 and 316 cm^{-1}) during the aggregation of $TPPS_4$ after the addition of spermine. Dashed line indicates the onset of the formation of the J aggregates (the appearance of the RLS signal) which grow according to a DLA mechanism. The inset reports the Raman spectrum collected 100 s after mixing the reagents.

portional to the enhanced Rayleigh scattering is derived, as explained in Ref. [31]. The frequency shifts in the low-frequency Raman spectrum of the $TPPS_4$-spermine composite, shown in the inset of Fig. 3, are very similar to that reported in the literature for the aggregated diacid $TPPS_4$. In particular, the two bands at 242 and 316 cm^{-1} were previously assigned to vibrational motions of the aggregated porphyrin [10]. The time evolution of these two bands, just after adding spermine to the aqueous solution of the porphyrin, evidences that this process is complete in about 60 s (see Fig. 3).

The same process has been investigated using fluorescence emission: the typical two-band emission of the diacid monomeric porphyrin is quenched upon aggregation. Figure 4 displays the kinetic evolution of the emission intensity at 700 nm together with that of the Raman intensity; as can be seen, the kinetic traces obtained from the two techniques are complementary. It is worth noting that the fluorescence emission in the composite, which is expected to be enhanced as well as the Rayleigh and Raman scattering, is quenched because of porphyrin aggregation.

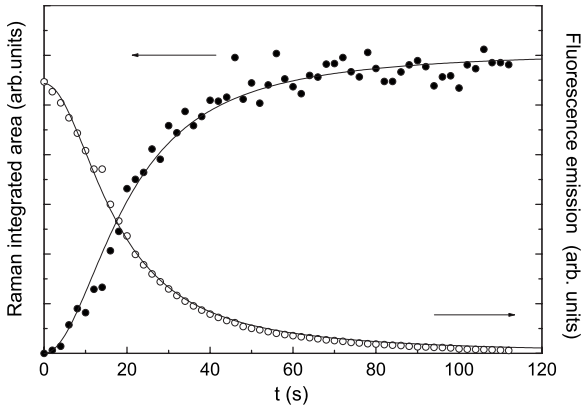

FIG. 4. Kinetic profile of the fluorescence emission and of the Raman integrated area (data of Fig. 3) for the aggregation of $TPPS_4$ after the addition of spermine. The continuous lines are the fit curves according to Eq. (3) with $a^2\epsilon$=0.01 s^{-2}.

During this initial stage (within about 60 s from mixing), fluorescence quenching occurs together with a huge increase of the Raman peak amplitude, indicating that porphyrin monomers form aggregates. The flat Rayleigh scattering profile and the absence of RLS signal suggest that aggregates are rather small during this early stage. Afterward, the crossover toward an almost constant Raman scattered intensity and the appearance of the RLS band suggest the triggering of the typical kinetics (tens of hours), leading to larger aggregates (DLA) whose size reaches a few micrometers. Both the mean-field theoretical approach based on the von Smoluchowski equation [22] and MD simulation results [23] suggest that a DLA regime is preceded by a clustering kinetic process according to a RLA mechanism. In fact, since the sticking probability between monomers is very low, at the beginning of the process only small clusters are formed. Thereafter, these small clusters give rise to bigger aggregates whose sticking probability increases on increasing their relative size. Only when the cluster probability becomes close to unity does the DLA mechanism occur. Depending on the thermodynamic parameters of the solution and on the investigating technique, this early RLA stage can be difficult to detect. For example, uv-visible measurements indicated that an initial exponential decay must be introduced to take into account the decrease of the monomer concentration [26]. Monomer depletion can be monitored in real time by the fluorescence quenching (porphyrin aggregates do not emit) or by the increasing intensity of the aggregate vibrational bands. Both Raman and fluorescence spectroscopy are effective tools to probe the porphyrin structural arrangements and the intermolecular interactions in the early stage of aggregation.

Di Biasio *et al.* [24] modified the von Smoluchowski equation to describe the transition region from the RLA to the DLA regime, introducing the following form for the kernel, which takes into account the low sticking probability of monomers:

$$K(i,j) = \begin{cases} \epsilon p_s & \text{for } i = j = 1, \\ p_s & \text{for } i,j \neq 1, \end{cases} \tag{2}$$

where p_s is the sticking probability and $0 \leqslant \epsilon \leqslant 1$. The analytical solution of Eq. (1) obtained for monomers becomes

$$c_1(t) \propto [4 + 4\epsilon at + \epsilon(at)^2]^{-1} \cong [4 + \epsilon(at)^2]^{-1}, \tag{3}$$

with at a scaled adimensional time depending on p_s and on the initial monomer concentration; the linear term is neglected since $at \gg 1$ (in the present case the linear term is at least three orders of magnitude smaller than the quadratic term).

Since the fluorescence intensity is proportional to $c_1(t)$ and the Raman intensity to $c_1(0) - c_1(t)$, both the experimental data sets in Fig. 4 were fitted by using Eq. (3); the continuous lines represent the fit results obtained with the same values of the parameter $a^2\epsilon$ [38]. Therefore, both these experimental findings point to the presence of an early stage of

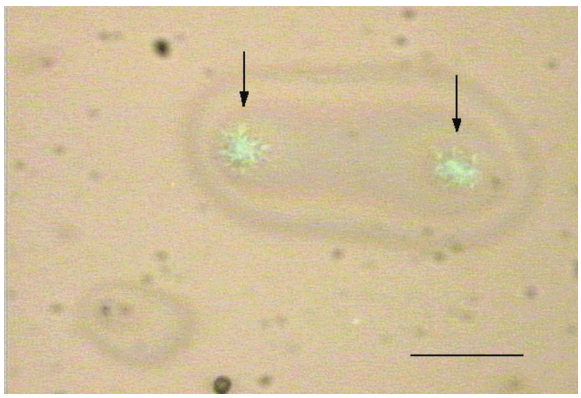

FIG. 5. (Color online) Optical microscopy image of a sample of $TPPS_4$-spermine composite deposited on a glass cover slide after evaporating the solvent. (The bar is 10 μm; for the experimental conditions see text.) The arrows indicate the fractal $TPPS_4$-spermine clusters.

the aggregation kinetics, in which small aggregates need to be formed. This early stage can be related to the expected RLA regime.

The induction time observed in the uv-visible and RLS kinetic profiles, which has also been reported for this porphyrin in the absence of templating reagents [39] and for other aggregating porphyrins [26,40], could be due to the nondetectable RLA initial stage.

The peculiar features of the $TPPS_4$-spermine composite are further evidenced in micro-Raman spectra of samples dried after the DLA aggregation process is completed (micrometric-sized fractals). The optical image reported in Fig. 5 clearly shows the presence of discrete objects having a dendriticlike morphology and sizes of a few micrometers. Moreover, Fig. 6 shows the presence of the bands at 242 and 316 cm^{-1} already found in solution in the low-frequency Raman spectrum.

These results suggest that both the structural and vibrational dynamical features of the composite in solution remain unchanged in the dried sample. A micro-Raman map of the

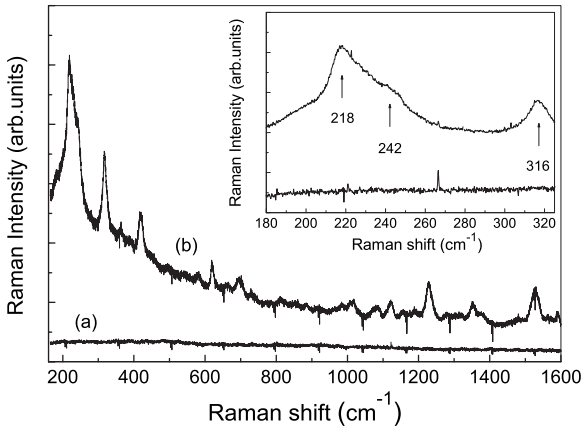

FIG. 6. Micro-Raman spectra of the deposited sample [(a) outside and (b) inside the fractal cluster]. In the inset the low-frequency region is reported.

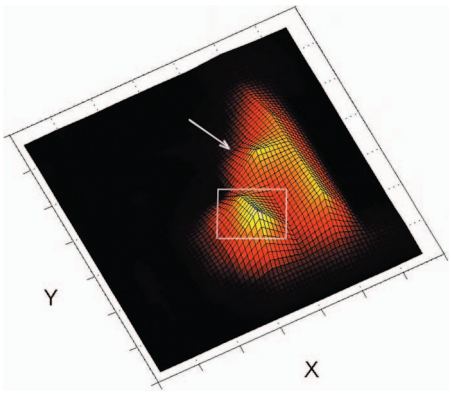

FIG. 7. (Color online) Micro-Raman image collected as intensity at 242 cm^{-1} for the spermine-induced $TPPS_4$ aggregates deposited on glass. The explored surface is 7×7 μm^2. Brighter zones represent higher Raman intensity. The arrow denotes a branch of the cluster and the box indicates a region in which the hot zones are averaged out because of the micrometric spatial resolution of the experimental apparatus.

intensity at 242 cm^{-1} was collected and is reported in Fig. 7 for a generic cluster (whose Rayleigh image is shown in Fig. 5). Due to the lack of translational invariance of fractal composites, excitation and scattered Stokes fields are localized in subwavelength regions, called hot zones. The low resolution of the micro-Raman spectroscopy (about 1 μm) prevents us from distinguishing the single inhomogeneities of the localized field. However, Fig. 7 clearly shows the spatial distribution of the Raman intensity in a single cluster (also along its branches), whereas the intensity of the hot zones is averaged out. Finally, Fig. 6 shows that a new strong band at 218 cm^{-1} appears; an inspection of the Raman spectrum of the polyamine alone in solution (at higher concentration) in this region excludes the possible assignment of this band to a neat spermine molecule vibration. Instead, it could be likely attributed to vibrations of spermine aggregates induced by the evaporation of the solvent.

V. CONCLUSION

Rayleigh and Raman (low-frequency range) light scattering measurements allow us to determine structural and vibrational features of $TPPS_4$ aggregates induced by spermine. The addition of this polyamine, at *p*H values fairly high with respect to those needed for aggregation in the absence of a templating reagent, triggers an aggregation process whose growth mechanism (DLA) leads to fractal clusters with size up to a few micrometers.

The time evolution of the enhanced Raman band intensity and the parallel quenching of fluorescence emission intensity during the initial aggregation process indicate that remarkable changes occur in the first stage when small clusters are likely to be formed.

In the $TPPS_4$-spermine composite the scattering enhancement aids the identification of the early stage of the porphyrin aggregation; this stage is reasonably attributable to a reaction-limited aggregation mechanism, which is expected to precede the diffusion-limited step responsible for the final observed structure.

[1] J. M. Lehn, *Supramolecular Chemistry* (VCH, Weinheim, 1995).
[2] W. I. White, in *The Porphyrins*, edited by D. Dolphin (Academic Press; New York, 1978), Vol. 5, Chap. 7; C. A. Hunter and M. K. J. Sanders, J. Am. Chem. Soc. **112**, 5525 (1990); K. Kano, H. Minamizono, T. Kitae, and S. Negi, J. Phys. Chem. **101**, 6118 (1997).
[3] M. D. Ward, Chem. Soc. Rev. **26**, 365 (1997); T. Hayashi and H. Ogoshi, *ibid.* **26**, 355 (1997); L. Monsù Scolaro, M. Castriciano, A. Romeo, N. Micali, N. Angelini, C. Lo Passo, and F. Felici, J. Am. Chem. Soc. **128**, 7447 (2006).
[4] *Photodynamic Therapy, Basic Principles and Clinical Applications*, edited by B. W. Henderson and T. J. Dougherty (Marcel Dekker, New York, 1992).
[5] R. F. Pasternack and E. J. Gibbs, in *Metal Ions in Biological Systems*, edited by A. Sigel and H. Sigel (Marcel-Dekker, New York, 1996), Vol. 33.
[6] H. S. Nalwa, in *Nonlinear Optics of Organic Molecular and Polymeric Materials*, edited by H. S. Nalwa and S. Miyata (CRC Press, Boca Raton, FL, 1997), p. 611; E. Collini, C. Ferrante, and R. Bozio, J. Phys. Chem. B **109**, 2 (2005).
[7] O. Ohno, Y. Kaizu, and H. Kobayashi, Chem. Phys. **99**, 4128 (1993).
[8] R. F. Pasternack, K. F. Schaefer, and P. Hambright, Inorg. Chem. **33**, 2062 (1994).
[9] J. M. Ribó, J. Crusats, J. A. Farrera, and M. L. Valero, J. Chem. Soc., Chem. Commun. **(1994)**, 681.
[10] D. L. Akins, S. Ozcelik, H. R. Zhu, and C. Guo, J. Phys. Chem. **100**, 14390 (1996); D. L. Akins, H. R. Zhu, and C. Guo, *ibid.* **100**, 5420 (1996).
[11] B. Ren, Z. Q. Tian, C. Guo, and D. L. Akins, Chem. Phys. Lett. **328**, 17 (2000).
[12] J. M. Ribó, J. Crusats, F. Sagues, J. Claret, and R. Rubires, Science **292**, 2063 (2001).
[13] S. C. M. Gandini, E. L. Gelamo, R. Itri, and M. Tabak, Biophys. J. **85**, 1259 (2003).
[14] N. Micali, F. Mallamace, A. Romeo, R. Purrello, and L. Monsù Scolaro, J. Phys. Chem. B **104**, 5897 (2000).
[15] M. A. Castriciano, A. Romeo, V. Villari, N. Micali, and L. Monsù Scolaro, J. Phys. Chem. B **107**, 8765 (2003).
[16] L. Monsù Scolaro, A. Romeo, M. Castriciano, and N. Micali, Chem. Commun. (Cambridge) **(2005)**, 3018.
[17] M. A. Castriciano, A. Romeo, V. Villari, N. Micali, and L. Monsù Scolaro, J. Phys. Chem. B **108**, 9054 (2004).
[18] M. A. Castriciano, A. Romeo, V. Villari, N. Angelini, N. Micali, and L. Monsù Scolaro, J. Phys. Chem. B **109**, 12086 (2005).
[19] S. M. Andrade and S. M. B. Costa, Chem.-Eur. J. **12**, 1046 (2006).
[20] N. Micali, A. Romeo, R. Lauceri, R. Purrello, F. Mallamace, and L. Monsù Scolaro, J. Phys. Chem. B **104**, 9416 (2000).
[21] N. Micali, V. Villari, M. Castriciano, A. Romeo, and L. Monsù Scolaro, J. Phys. Chem. B **110**, 8289 (2006).
[22] F. Leyvraz and H. R. Tscudi, J. Phys. A **14**, 3389 (1981).
[23] P. Meakin, T. Vicsek, and F. Family, Phys. Rev. B **31**, 564 (1985).
[24] A. Di Biasio, G. Bolle, C. Cametti, P. Codastefano, F. Sciortino, and P. Tartaglia, Phys. Rev. E **50**, 1649 (1994).
[25] T. Vicsek and F. Family, Phys. Rev. Lett. **52**, 1669 (1984).
[26] F. Mallamace, L. Monsù Scolaro, A. Romeo, and N. Micali, Phys. Rev. Lett. **82**, 3480 (1999).
[27] V. M. Shalaev, Phys. Rep. **272**, 61 (1996).
[28] M. I. Stockman, Phys. Rev. E **56**, 6494 (1997).
[29] M. I. Stockman, L. N. Pandey, and T. F. George, Phys. Rev. B **53**, 2183 (1996).
[30] M. I. Stockman, V. M. Shalaev, M. Moskovits, R. Botet, and T. F. George, Phys. Rev. B **46**, 2821 (1992).
[31] N. Micali, V. Villari, L. Monsù Scolaro, A. Romeo, and M. A. Castriciano, Phys. Rev. E **72**, 050401(R) (2005).
[32] L. D. Bakalis and J. Knoester, J. Lumin. **87**, 66 (2000).
[33] M. Vacha, M. Furuki, L. S. Pu, K. I. Hashizume, and T. Tani, J. Phys. Chem. B **105**, 12226 (2001).
[34] R. F. Pasternack and P. J. Collings, Science **269**, 935 (1995).
[35] P. G. Gucciardi, S. Trusso, C. Vasi, S. Patanè, and M. Allegrini, in *Applied Scanning Probe Methods V*, edited by B. Bhushan, H. Fuchs, and S. Kawata (Springer-Verlag, Berlin 2007), Chap. 10.
[36] N. C. Maiti, M. Ravikanth, S. Mazumdar, and N. Periasamy, J. Phys. Chem. **99**, 17192 (1995); J. M. Ribó, R. Rubires, Z. El-Hachemi, J. A. Farrera, L. Campos, G. L. Pakhomov, and M. Vendrell, Mater. Sci. Eng., C **11**, 107 (2000).
[37] H. E. Stanley and N. Ostrowsky, in *On Growth and Form*, edited by H. E. Stanley and N. Ostrowsky, NATO Advance Studies Institute (Martinus Nijhoff Publishers, Dordrecht, 1986).
[38] It is to be noticed that a fitting with an exponential law does not furnish results as good as Eq. (3).
[39] R. F. Pasternack, C. Fleming, S. Herring, P. J. Collings, J. dePaula, G. DeCastro, and E. J. Gibbs, Biophys. J. **79**, 550 (2000).
[40] R. F. Pasternack, E. J. Gibbs, P. J. Collings, J. C. dePaula, L. C. Turzo, and A. Terracina, J. Am. Chem. Soc. **120**, 5873 (1998).